



Rapid and portable mid-infrared analysis of wet sediment samples by a novel “filter-press” attenuated total reflectance method

Leslie J. Janik^{1,2} · Stuart L. Simpson³ · Mark Farrell⁴ · Luke M. Mosley²

Received: 31 May 2023 / Accepted: 29 November 2023 / Published online: 4 January 2024
© Crown 2024

Abstract

Mid-infrared (MIR) analysis of wet sediments or soils usually requires freezing and drying, adding considerable analysis time and cost, and promoting changes in chemical properties. A novel attenuated total reflectance (ATR) mid-infrared (MIR) method was developed to enable analysis of non-processed, aqueous sediments. Wet sediment samples from the Coorong Lagoon, South Australia, were subjected to laboratory analysis for physical and chemical properties, our new filter-press ATR method, and conventional ATR and diffuse reflectance (DRIFT) analysis of dried samples. For ATR on wet sediments, samples were pressed onto the ATR crystal with a filter-paper backing and scanned. The spectra were analyzed by principal components analysis (PCA) and partial least squares regression (PLSR) to develop multivariate models for total organic carbon (TOC). ATR spectra of as-received wet sediments were poor due to water absorption features, but filter-pressing reduced these and greatly enhanced the solids spectral component. The filter-pressed PLSR cross-validation for TOC resulted in an $R^2=0.89$ and $RMSECV=0.78\%$. Prediction accuracies were similar to freeze-dried ATR samples and far more accurate than testing wet samples without filter-pressing. Our findings confirmed the filter-press ATR method as proof-of-concept and showed that it has the potential to remove one of the major barriers to in-field application of MIR techniques, the high and variable amounts of moisture levels commonly present in many environmental samples. Extension of the filter-press ATR method to a wider range of analytes may enable it to rapidly acquire moist or wet sediment and soil property data while in the field.

Keywords Saturated sediments · ATR · MIR · On-site analysis · PLSR

Introduction

Since the introduction of infrared techniques for soil analysis, numerous studies have reported the successful prediction of a wide range of soil properties such as organic carbon (OC) and its fractions (Janik and Skjemstad 1995; Janik et al. 2007; Baldock et al. 2013; McCarty and Reeves 2006; Reeves 2010; McCarty et al. 2002; Viscarra Rossel

et al. 2006; Zimmermann et al. 2007; Soriano-Disla et al. 2014). These analyses have generally used the mid-infrared (MIR) diffuse reflectance infrared (DRIFT) technique on dried < 2 mm sieved soil samples or finely ground powders. Dry samples are required for MIR DRIFT because when moist or wet samples are scanned, spectral distortion and band intensity reduction due to specular reflection from the surface water can occur and can severely reduce the regression modeling accuracies. Furthermore, sample heterogeneity in unground or coarsely ground samples has presented problems in MIR analysis due to surface reflections of the infrared beam from large particle or aggregate surfaces (Janik et al. 2016a). Scanning completely wet samples by MIR DRIFT is, therefore, not feasible.

This distortion is far less in the visible and near infrared (vis–NIR) region due to the lower spectral intensities and therefore lower reflection effects, so that vis–NIR spectroscopy can be suitable for wet samples (Janik et al. 2016b). However, the vis–NIR produces much weaker and less

✉ Leslie J. Janik
les.janik@csiro.au

¹ CSIRO Environment, Kurna Country, Waite Road, Urrbrae, South Australia, Australia

² School of Biological Sciences, University of Adelaide, Kurna Country, Adelaide, South Australia, Australia

³ CSIRO Environment, Tharawal Country, Lucas Heights, New South Wales, Australia

⁴ CSIRO Agriculture and Food, Kurna Country, Waite Road, Urrbrae, South Australia, Australia

selective peaks for many minor soil organic matter groups and is insensitive for many silicate minerals, whereas the MIR is sensitive to a much broader range of soil components, the peaks are sharper and less overlapped, bringing more information compared to the vis–NIR. There is, therefore, an advantage in using an MIR technique if the moisture effects can be overcome.

There has been previous work using infrared techniques for analysis in aquatic systems, for example in lakes (Rosén et al. 2010), deltas (Chapkanski et al. 2020, 2022), watersheds (Poulenard et al. 2009), and marine environments (Hahn et al. 2016). Soils and sediments in these environments appear to have only previously been analyzed as dry powders by hyperspectral vis–NIR spectroscopy (Cohen et al. 2005), on intact cores (Shi et al. 2014), and also as dry powders by MIR DRIFT spectroscopy (Rosén et al. 2010; Soriano-Disla et al. 2019; Barros et al. 2022; Poulenard et al. 2009). However, drying of wet sediments or soils in some oxidative environments can result in changes or losses to chemical forms (e.g., speciation) of analytes. For example, in samples taken from locations with reducing environmental conditions, drying may promote oxidation of sulfidic phases, acidification and metal release (Creepers et al. 2013; Bargrivan et al. 2018; Mosley et al. 2019). Oxidation of nutrient-enriched wet samples may also result in transformation of the nutrient species (Turner et al. 2007; Kresović et al. 2010). It would, thus, be a considerable advantage if wet, samples, that may be sensitive to oxidation or other reactions with the atmosphere, could be analyzed in their natural state without drying. Furthermore, the elimination of the need for freezing, transporting, and drying samples prior to analysis would have a significant time and cost advantage.

An alternative MIR technique to DRIFT, intended to reduce the problems of analyzing wet samples, uses attenuated total internal reflectance (ATR) (Milosevic 2004; Griffiths and De Haseth 2007; Larkin 2018). Briefly, in ATR, the infrared beam is reflected internally from a high refractive index transparent crystal such as diamond, in contrast to external reflection directly from the sample surface as in DRIFT. Part of the reflected ATR beam penetrates through the surface of the crystal to a small distance beyond the surface. It is this infrared evanescent wave which is absorbed by the sample in close contact with the ATR crystal, resulting in the infrared spectrum. The depth of MIR penetration into common powdered minerals such as kaolinite is in the order of about $0.55\ \mu\text{m}$ at $3000\ \text{cm}^{-1}$ (Weidler and Friedrich 2007), increasing to $\sim 1.0\ \mu\text{m}$ at $1400\ \text{cm}^{-1}$. The bulk of the sample, greater than a depth of the first few microns near the crystal surface, is not seen by the evanescent wave. Because of this shallow sampling depth of the infrared radiation, even intensely absorbing materials such as water, as in a wet sediment sample, do not exceed the detector limit and reliable spectra can still

be obtained. Thus, ATR has a potential major advantage over MIR DRIFT for spectral analysis of wet sediment samples. However, in aqueous media (such as slurry samples), sample signal is weak compared to the massive water peaks. This can reduce the ability of the ATR technique to provide good quantitative analysis for key parameters, including organic carbon and mineralogy.

The majority of studies on marine sediments using ATR spectroscopy have been on dried samples (Ehsani et al. 2001; Oudghiri et al. 2014; Melucci et al. 2019; Xuebin et al. 2019; Koçak et al. 2021), rather than wet as in their natural environmental state. A few ATR studies have reported on samples such as soil pastes. Robertson et al. (2013) suggested that several soil properties such as clay minerals and organic matter may be determined in wet samples using ATR. They compared “wet soil” ATR spectra under wet, field conditions using a handheld MIR FTIR, recorded initially by smearing the sample onto the ATR crystal using a spatula, and by using a gloved hand to produce a thin smear which dried very quickly and closely resembled dry spectra. For OC, their cross-validation prediction for the “wet smear” spectra was relatively poor ($R^2 = 0.68$ and $\text{RMSECV} = 3.7\%$). Cross-validation for the dried “wet smear” dried spectra was far better ($R^2 = 0.98$ and $\text{RMSEP} = 0.87\%$). While promising, the timescale for drying of saturated sediment samples on the ATR crystal could be excessive, depending on ambient weather conditions, and would not be suitable for oxidation sensitive samples. The only study on the analysis of completely wet soils by MIR ATR that we have found focused only on the ionic concentrations of nitrate in the soil solution, rather than other soil properties (Shaviv et al. 2003; Linker et al. 2004, 2005).

When wet sediment samples are directly deposited onto an ATR crystal surface, most of the spectral signal is from water in contact with the ATR crystal, and with only a weak contribution from the relatively few dispersed solid sediment particles close to the crystal surface. However, by pressing the wet sediment sample against the ATR crystal surface with an absorbing backing such as filter paper, a compressed plug of concentrated sediment material is firmly pressed into optical contact with the crystal surface. The potential advantages from utilizing such a method would be a lower contribution of water in the infrared spectrum, more solid material within the influence of the evanescent wave and improvements in analyte prediction performance. As such, the proposed method is generalizable to other wet sediment or soil environments and is also potentially applicable to rapid field-based MIR analyses. The aim of this study was to demonstrate the filter-press ATR measurement technique as proof-of-concept, in order to provide a method for reliable quantitative analyses of wet sediments.

Methods

Samples

Wet sediment samples were collected along an estuarine lagoon, the Coorong in southern South Australia, with wide variations in salinity, organic and inorganic carbon, and nutrient and sulfide content (Priestley et al. 2022; Mosley et al. 2023). A sample site location map is provided in the Supplementary Information S1 along with more detailed information on the Coorong study area, using information provided by a number of authors (Mosley et al. 2020, 2023; Merry and Fitzpatrick 2005; Gingele and De Deckker 2005). The wide gradient in chemical properties made the Coorong a useful system to help test and validate the new ATR method.

A total of 37 wet sediment samples (calibration Set-1 with 26 samples for model development (C1–C26) and Set-2 with 11 samples for testing the model (T1–T11)) were collected. The test strategy, as implemented here, was designed to provide a realistic indication of the potential of the calibration set, as it is at present, to predict samples in the future. We acknowledge that a gradient method, rather than a separate samples test set would give a better prediction result. However, when the number of samples between the two sets are compared, 100% of the test set and 73% of the calibration sets had similar TOC values. The test as implemented here was considered to be a more realistic and rigorous and realistic one, even if it is showing less accuracy than a gradient selection method. Set-1 had been collected as described by Priestley et al. (2022) from locations depicted in Fig. S1. These sediment samples were taken from below approximately 1 m of water using a “Russian D” auger to a depth of approximately 50 cm (illustrated in Figs. S2 and S3). Some shallow shoreline samples were collected with a polycarbonate core tube pushed into the sediment. Set-2 samples were collected on a subsequent sampling date (March 2022) from Parnka Point (Sediments T1 and T2), Parnka South (Sediments T3–T6) and Tea Tree (Sediments T7–T11) (locations depicted in Fig. S1) under the same conditions as Set-1, with polycarbonate core tubes pushed into the sediments to a depth of approximately 50 cm. Sub-samples of the surface (0–5 cm) sediment layer were placed in sealed vials with no air gap and cooled on ice. Upon return to the laboratory (within 48 h), the samples were frozen at $-20\text{ }^{\circ}\text{C}$ until laboratory analysis.

A small set of reference materials, to test the possible impact on the spectra from the filter-paper backing, were also scanned to confirm if there was any spectral evidence of the filter-paper backing resulting from the filter-pressed method. These reference materials were Whatman #5 filter

paper, a low-crystallinity kaolinite clay (from Birdwood, South Australia), calcite (as calcium carbonate) from Merck, and a red Dermosol soil, high in kaolinite from Kingaroy (QLD, Australia).

Analytical reference data

Wet chemical analyses for calibration and validation of the ATR method were carried out by a NATA accredited laboratory (Environmental Analysis Laboratory, Lismore, NSW). Sub-samples were dried and ground upon receipt at laboratory and reported as dry weight. Moisture Content (% moisture) was determined on a separate wet sub-sample by loss of mass via drying at $105\text{ }^{\circ}\text{C}$. The Hydrometer Analysis method was used to determine the percentage sand, silt, and clay, via California Dept of Pesticide Regulation SOP meth004 modified by Gee and Bauder (1986). The texture classification was based on the hydrometer results and the appropriate texture triangle. pH, and Electrical Conductivity (EC) were measured on a 1:5 soil:water extract (Rayment and Lyons 2011, methods 4A1 and 4B1, respectively). Total phosphorus was determined via the Rayment and Lyons (2011) total acid extractable P method, total carbon (%TC), and total nitrogen (%TN) by LECO CNS TruMAC Analyser, %TOC after HCl-acid treatment by LECO CNS TruMAC Analyser, and total inorganic carbon (%TIC from carbonate) by calculation (%TC–%TOC). Samples for chromium reducible sulfur (CRS) were dried and ground immediately upon arrival, while samples for acid volatile sulfur (AVS) were analyzed wet and corrected to dry weight using the moisture content. Analytical procedures for CRS and AVS were sourced from Sullivan et al. (2018). Laboratory data for the Set-1 (calibration sediments) and Set-2 (model testing sediments) are provided in Table 1, and additional data and geolocations and sampling depth provided in Tables S1 (Set-1) and Table S2 (Set-2). Laboratory analyses for carbonate, clay, sand, and metals were not determined for Set-2.

Spectroscopy

Spectra were collected with an Alpha mid-infrared FTIR spectrometer (Bruker Inc. USA). Schematic diagrams of the filter-press ATR mechanism, showing the effect of compressing the sample onto the ATR crystal are presented in Figs. 1a and 1b. The ATR accessory (Fig. 1c), the anvil pressing on the filter paper with the sample (Fig. 1d), the pressed sample on the underside of the filter paper (Fig. 1e), and upper surface of the filter paper after pressing (Fig. 1f) are also shown.

Each Set-1 sample was scanned in the MIR in four modes: as-received ATR, filter-paper pressed ATR (model calibration), freeze-dried ATR, and freeze-dried DRIFT. The eleven Set-2 samples were only scanned with the filter-paper

Table 1 Laboratory data for sediment properties

Sediment	ID	MOISTURE (%)	TOC (%)	TIC (%)	CLAY (%)	TP (mg/kg)	TN (%)	AVS (%)
<i>Set-1 (Calibration): Sediments from the Coorong</i>								
C1	1	28.8	0.26	8.36	7	163	0.05	0
C2	3	19.3	0.30	7.1	5	171	0.04	0
C3	4	80.4	6.36	3.74	57	547	0.78	0.02
C4	7	79.3	6.31	3.03	70	504	0.75	0.05
C5	9	80.6	6.64	2.68	79	688	0.78	0.04
C6	12	36.8	0.82	5.24	11	130	0.14	0
C7	15	80.1	5.55	2.28	82	522	0.72	0.05
C8	16	66.9	2.97	5.19	35	422	0.38	0.04
C9	17	71.3	3.90	1.87	51	371	0.45	0.07
C10	20	80.2	5.94	1.29	92	580	0.75	0.06
C11	23	80.8	5.16	1.36	90	685	0.7	0.05
C12	26	74.3	2.58	4.65	82	373	0.46	0.06
C13	27.1	18.4	0.30	0.06	4	47	0.05	<0.001
C14	27.2	18.6	0.18	0.19	2	21	0.03	0
C15	27.3	25.2	0.13	0.06	3	23	0.03	0.01
C16	28	21.1	0.39	0.15	5	64	0.05	0.01
C17	29	29.9	0.82	0.83	15	79	0.1	0.04
C18	30	38.6	0.96	2.0	20	89	0.09	0.01
C19	31	58.4	2.63	2.2	39	331	0.31	0.08
C20	32	26.1	0.71	0.81	7	73	0.07	0.02
C21	33	27.7	0.75	0.71	10	84	0.08	0.02
C22	34	21.6	0.35	3.18	6	58	0.06	0.01
C23	35	77.4	5.55	0.41	83	528	0.68	0.08
C24	40	42.3	1.26	0.21	16	166	0.17	0.05
C25	45	64.8	1.67	1.15	50	281	0.24	0.05
C26	50	42.3	1.09	0.42	11	215	0.13	0.04
<i>Set-2 (Model testing): Sediments at Parnka and Tea Tree</i>								
T1	101-1		4.91			665	0.69	0.068
T2	101-2		2.2			337	0.29	0.04
T3	102-1		1.14			180	0.14	0.006
T4	102-2		0.70			133	0.08	0.001
T5	102-3		2.35			288	0.27	0.011
T6	102-4		0.75			183	0.09	0.002
T7	103-1		0.83			94	0.11	0.001
T8	103-2		0.73			98	0.08	0.002
T9	103-3		0.63			52	0.07	0.001
T10	103-4		0.59			59	0.06	0.001
T11	103-5		0.89			118	0.11	-0.003

Additional sediment properties data, including pH, EC, Texture, % silt and sand, Chromium Reducible Sulphur (CRS) is provided in Table S1 of the Supplementary Information

pressed method (model testing). For the as-received ATR method, subsamples (approx. 2 g) of Set-1 were taken from the frozen vials in the laboratory, thawed and hand-homogenized in an agate mortar for 20 s. From this homogenized sub-sample, a small amount of the wet homogenate (approx. 0.2 g) was placed onto the surface of a single-bounce diamond ATR crystal and scanned.

After the initial scan of the wet homogenate, a filter paper (No. 5, Whatman) was folded into quarters, placed over the wet sample on the ATR crystal, pressed against the diamond crystal with the ATR accessory anvil, and re-scanned (Fig. 1d). The diamond ATR anvil applies a set pressure of approximately 18 kg onto the 2.5 mm² diamond surface. This method is described hereafter as the ‘filter-press’

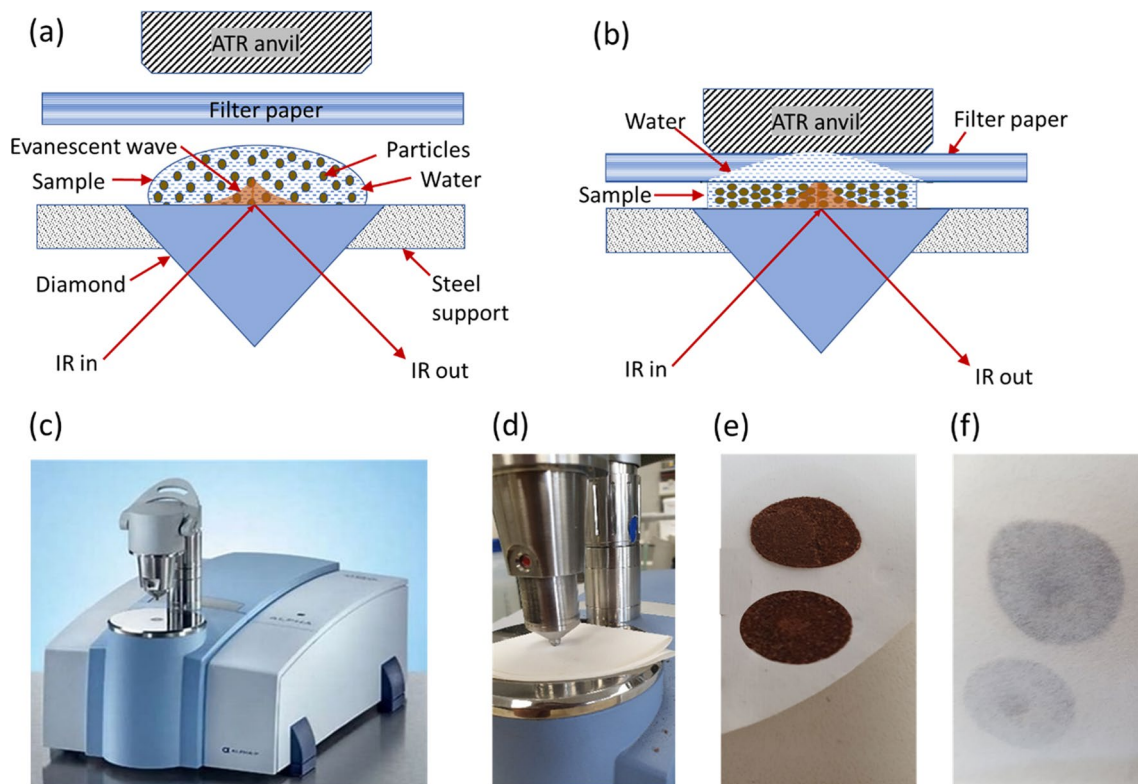


Fig. 1 Schematic diagram of the ATR method for wet samples. **a** ATR crystal with wet soil added to the surface, and **b** the sample pressed against the crystal surface at high pressure with a filter-paper backing. The evanescent wave is the portion of the infrared beam that extends into the space just beyond the crystal surface and is dependent on the angle of incidence, refractive index of the crys-

tal, and refractive index of the sample (Weidler and Friedrich 2007). **c** Bruker FTIR spectrometer with single-bounce diamond ATR, **d** sample pressed onto diamond crystal with filter paper, **e** sample plug on underside of filter paper, and **f** moisture on upper surface of filter paper absorbed from sample. The labels C13 and C17 refer to samples with low moisture effects

method. The pressed sample plugs on the underside of the filter paper, in contact with the ATR crystal, are shown in Fig. 1e, and the upper surface of the filter paper with the removed moisture is shown in Fig. 1f. Care was taken to ensure sufficient depth of the sediment plug to reduce any adverse interference from the filter-paper backing. Excess quantity of material was not important since only the first few microns are detected by ATR. Each sample was scanned for 100 s in the range $4000\text{--}400\text{ cm}^{-1}$ at an 8 cm^{-1} resolution. Duplicates were not taken.

Sub-samples of Set-1, approximately 5 g, were placed into a Dynavac freeze-drier (Dynapumps, Melb. Aust.) and dried overnight. The freeze-dried samples were fine-ground for 20 s in an agate mortar and subsamples (approx. 0.1 g) were scanned directly on the ATR crystal under anvil pressure but without filter-paper backing. Comparative scans using the diffuse reflectance infrared (DRIFT) method, with the same Bruker spectrometer and using the freeze-dried samples, were carried out to ascertain how well the ATR method performed in comparison to the more common dried-powder DRIFT method. The small set of reference samples for testing the impact of filter paper on the spectra

were dry pressed onto the ATR crystal and scanned, and then pressed onto the crystal with the filter paper as 33% sample in deionized (Milli-Q) water and re-scanned.

As a cursory additional experiment, vis-NIR spectra of the wet Set-1 samples were scanned directly in reflectance mode, using an SM-3500 OreXpress (Spectral Evolution, MA, USA), in the spectral range 250–2500 nm. Vis-NIR was only carried out as an additional comparison with the filter-pressed ATR technique for possible interest by those more familiar with vis-NIR spectroscopy rather than the MIR.

Set-2 was scanned in the same manner as for the filter-pressed Set-1 samples. The homogenization and measurement process took only a few minutes per sample. To answer the questions about instrument field application, for this phase of the work, the spectrometer was powered through an inverter directly from a free-standing 12 V car battery rather than through mains power, emulating a field-use scenario. Tests showed that some instrument instability could result from restarting the spectrometer during a scanning regime, so that scanning was made for the complete set without restarting the spectrometer at any stage.

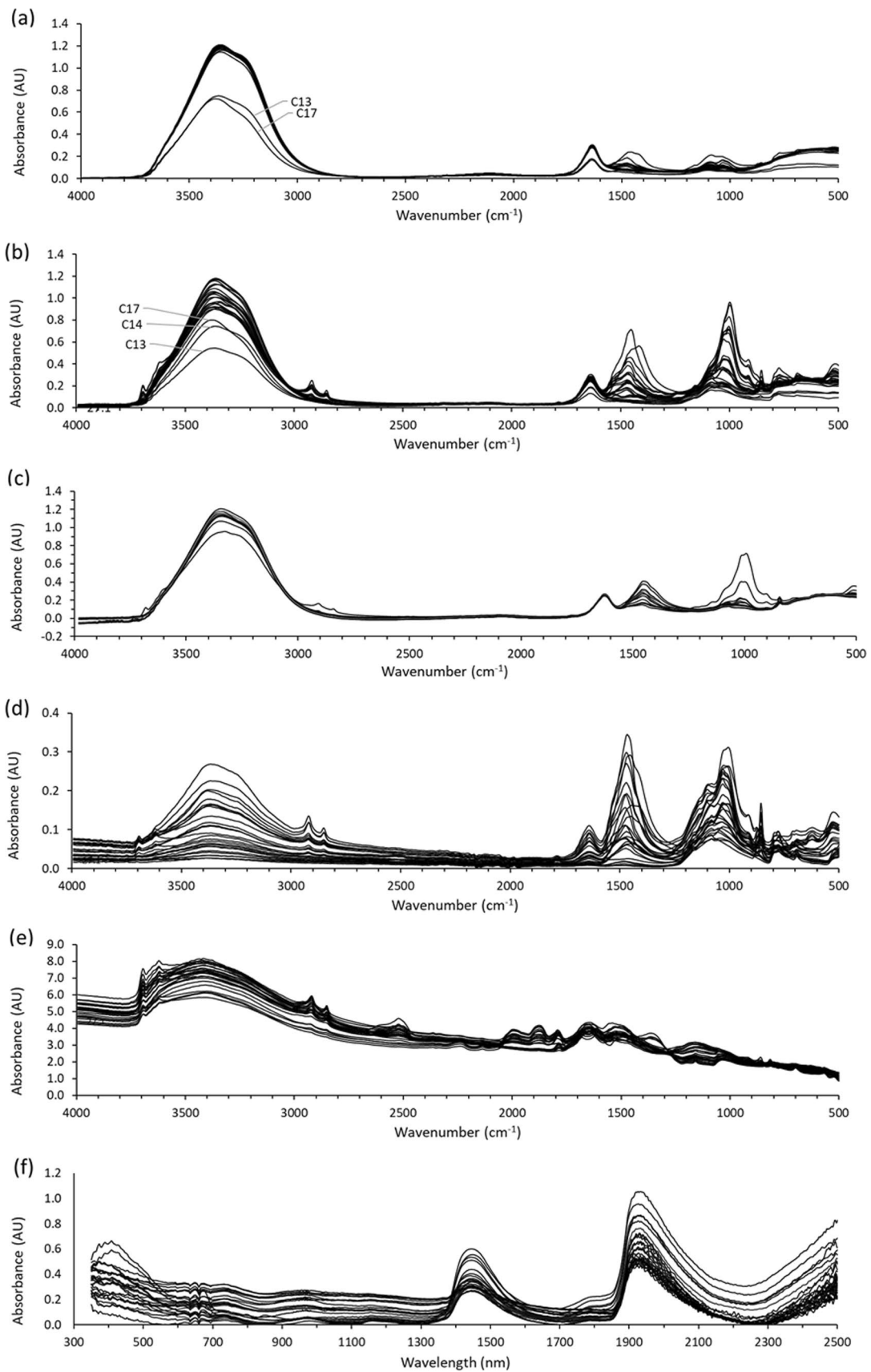


Fig. 2 MIR ATR spectra of the sample used in the study. Set-1 calibration sediment samples **a** as-received, **b** after pressing onto the ATR crystal with filter-paper backing, **c** spectra of the filter-pressed Set-2 samples, **d** freeze-dried powders pressed directly onto ATR crystal, **e** DRIFT of dried powders, and **f** vis-NIR reflectance. The labels C13, C14 and C17 refer to samples with low moisture effects

Chemometrics

The Bruker spectra were imported into the UnscramblerX v10.5 software (Camo, Trondheim, Norway) and pre-processed with a baseline offset correction. Principal components analysis (PCA) was carried out within Unscrambler. The PCA score plots for the spectrum set were used to assess the extent of spectral variance between within each sample set, and the PCA loadings used to describe the key spectral characteristics of the sample set. Major outliers were identified and omitted from the PCA analysis to remove extreme spectral characteristics that would disproportionately influence the models. Partial least squares regression analysis (PLSR) was carried out using the OPUS Quant-2 package, rather than Unscrambler, because of the automatic spectral preprocessing option available optimizing the PLSR models. PLSR models were trained using leave-one-out cross-validation to derive the optimum calibration models (Geladi and Kowalski 1986). The PLSR statistics were described by the R^2 , the RMSE (RMSECV for cross-validation and RMSEP for prediction), and the interquartile ratio of performance (RPIQ), where $RPIQ = IQ/RMSEP$ and IQ is the interquartile distance ($Q3 - Q1$). The RPIQ statistic is reported to give a better representation of the calibration robustness than the more commonly used RPD (ratio of standard deviation to RMSE), in that it does not include extreme analytical values that could heavily leverage the regression (Bellon-Maurel et al. 2010). We assumed model robustness according to RPIQ values < 1.5 as considered poor, $1.5 - 2.0$ indicator quality, $2.0 - 3.0$ suggest good quality, and > 3.0 considered analytical quality (Fearn 2001). In some cases, outliers were identified and omitted from the PLSR analysis where it was thought that they may have an undue leverage on the PLSR models.

Results

Spectra

Spectra of the as-received Set-1 field-wet samples, depicted in Fig. 2a, showed a strong, broad water absorption feature with a peak maximum varying between 3360 and 3340 cm^{-1} , an overlapped shoulder near 3270 cm^{-1} , and a band at 1630 cm^{-1} . The absorbance intensities near 3360 cm^{-1} were within a range of 1.14 absorbance units (AU), close to that

of pure water (~ 1.20 AU), for all samples except for the two outliers (sediments C13 and C17) with lower moisture contributions. This narrow range of water band intensities suggested that a film of water was spread from sample to ATR crystal surface, resulting in the dominant spectral absorbance with very little correlation with the large range of as-received moisture values (18.4–80.8%) (Table 1).

The spectral range $1600 - 950$ cm^{-1} was relatively weak compared to the water band but showed peaks mostly due to carbonate, silicate (possible quartz) and kaolinite clay (Nguyen et al 1991; Van der Marel and Beutelspacher 1976). There was no evidence of organic matter in the spectra of these as-received samples. Maximum band intensity for carbonate was 0.24 AU at 1460 cm^{-1} (sediment C2), 0.21 AU for quartz at 1085 cm^{-1} (sediment C16), and 0.17 AU for kaolinite at 1032 cm^{-1} (sediment C19). On average the maximum sediment intensities were approximately 20% of the water band. This observation supported the idea that the evanescent wave was impacted by only a small percentage of solids.

Following the filter-pressing process, the peaks in Fig. 2b exhibited a significant increase in spectral intensities within the $1600 - 950$ cm^{-1} region, indicating the detection of a greater variety of sediment components, as opposed to the as-received spectra shown in Fig. 2a. This enhancement amounts to a three–fivefold increase in intensity. The water band near 3360 cm^{-1} showed only slight-moderate reductions in absorbance intensities, with a range of 0.90 AU (sediment C7) to 1.18 AU (sediment C22) (except for the three outliers of sediments C13, C14 and C17), corresponding to an average water intensity reduction of 15%. The intense 1460 cm^{-1} peak for sediment C8, assigned to carbonate, increased threefold to 0.71 AU, and a number of strong bands were observed in the $1050 - 1000$ cm^{-1} region, assigned to silicate Si–O. In contrast to the as-received spectra, where there were no peaks observed for clay or organic matter in the $4000 - 2500$ cm^{-1} region, there was now a clearly observable peak at 3695 cm^{-1} for kaolinite, and two sharp peaks due to organic alkyl at 2920 and 2850 cm^{-1} .

The spectra of the filter-pressed, battery-powered, Set-2 samples (Fig. 2c) were of similar quality, although weaker, to that of Set-1. There were strong water bands between 3360 and 3340 cm^{-1} , a band at 1630 cm^{-1} and evidence of organic matter near $2930 - 2850$ cm^{-1} . The spectral range $1600 - 950$ cm^{-1} showed peaks mostly due to carbonate (1460 cm^{-1}) and kaolinite clay (doublet at $1032 - 1003$ cm^{-1}).

The ATR spectra of the freeze-dried powdered samples, depicted in Fig. 2d, showed that there were further strong reductions in water absorbance intensities near 3360 cm^{-1} , with a range of 0.03 AU (sediment C26) to 0.27 AU (sediment C4) absorbance units (AU), corresponding to an average reduction of 91% from the original as-received samples. Clearly, the water film on the crystal surface was now

almost absent, with only the solid material pressed onto the crystal. Peaks due to carbonate (0.34 AU for Sediment C8), quartz (0.22 AU for Sediment C4), and kaolinite (0.31 AU for Sediment C23) were again observed. However, there was a reduction in the overall ATR spectral intensities in the 1600–950 cm^{-1} spectral region, probably due to reduced optical contact by the presence of air between the sediment particles and crystal surface.

The diffuse reflectance (DRIFT) spectra on dried and ground samples shown in Fig. 2e were, as expected, completely different to the ATR. In DRIFT, there are strong effects from specular reflectance; the strong O–Si–O peaks being very weak and inverted compared to the ATR, and the very weak quartz combination/overtone peaks near 2000–1850 cm^{-1} now becoming observable (Janik et al. 2016b). Importantly, the carbonate overtone peak at 2517 cm^{-1} , observed in the usual application of MIR DRIFT analysis of carbonate analysis (Hume et al. 2022) and too weak to be observed in the ATR spectra, were now clearly discernible.

Spectra of the as-received Set-1 samples in the vis–NIR spectral region are depicted in Fig. 2f. Major broad bands due to –OH functional groups were observed at about 1450 and 1940 nm corresponding to water. Further spectral

variation occurred in the visible region, with a series of strong bands around 405 nm. A weak unassigned shoulder near 1790 nm, and other weak, broad bands were observed near 740, 950 and 1150 nm in some samples but could not be assigned. Quartz does not have a vis–NIR signature and there were no bands observed that could be unambiguously attributed to minerals such as carbonate (usually at 1690, 1900 and 2270 nm—Khayamim et al. 2015) or kaolinite (usually at 2200 nm—Demattê et al. 2015).

Principal components analysis (PCA)

Set-1

The spectral variability can be conveniently assessed from the PCA plots. Figure 3a depicts the score plots of the first two principal components (PCs) after filter-pressing. Samples C13, C14, and C17 appear to be outliers, separated from the other samples along negative PC1. The loadings for PC1 and PC2 depicted the major compositional components contributing to the spectra of the filter-pressed samples (Fig. 3b). An extended set of plots of the first four PCA loadings is depicted in Fig. S4 for further reference.

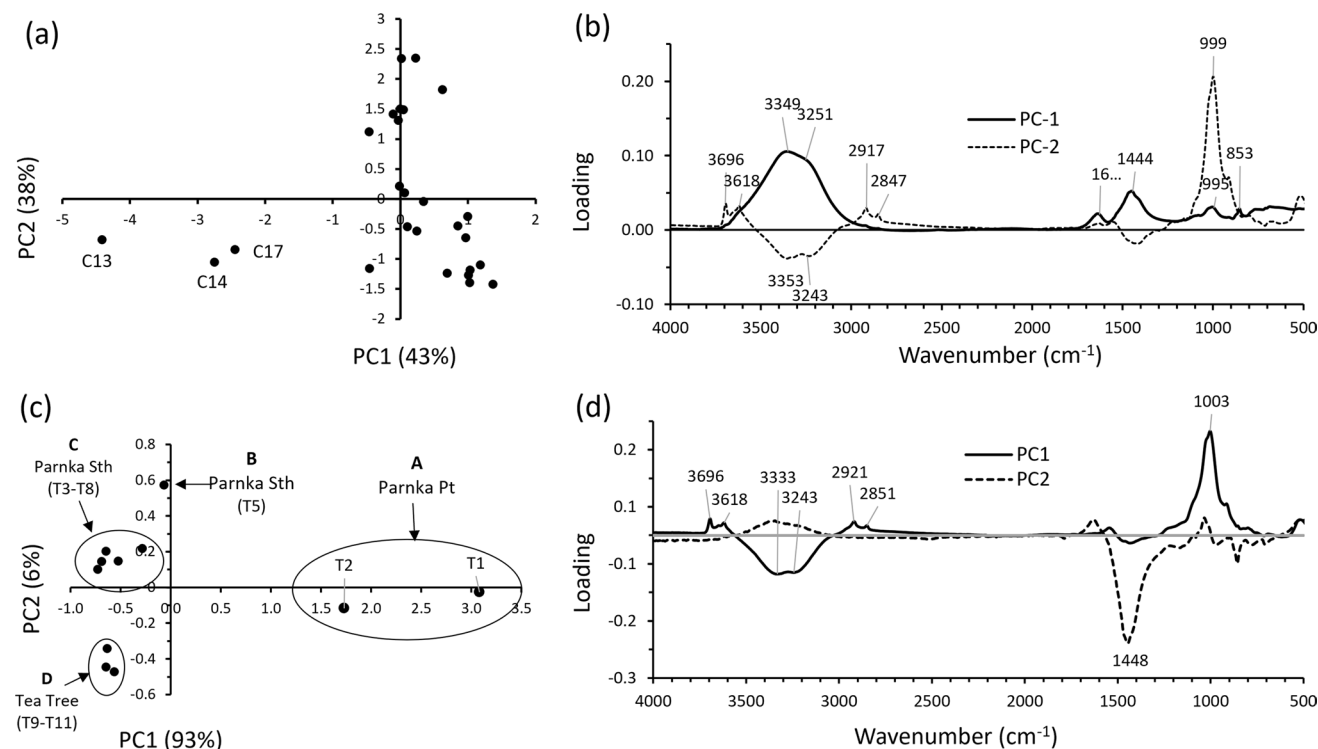


Fig. 3 PCA plots. **a** Set-1 scores after pressing wet sample onto the ATR crystal with filter-paper backing and **b** the PCA Loadings for PC1 and PC2. Outliers C13, C14 and C17 are shown in the Set-1 score plots. PCA plots shown for **c** Set-2 scores (PC1 and PC2), and

d Loadings. The score groupings A (sediments T1 and T2), B (T5), C (sediments T3, T4, T6, T7, and T8) and D (sediments T9–T11) are depicted for Set-2 samples in (c). The main peak labels are shown in the loading plots

PC1 loading was dominated by peaks due to water (3349–3251 cm^{-1}) and carbonate (as aragonite at 1444 and 853 cm^{-1}) (Jovanovski et al. 2002). The source of aragonite in the Coorong has been reported to precipitate directly out of solution due to hypersalinity and evapo-concentration of Ca^{2+} and CO_3^{-2} . PC2 loading was dominated by peaks due to organic carbon (2917–2847 cm^{-1}) and kaolinite clay (3696–3618 cm^{-1} and 999 cm^{-1}). This 999 cm^{-1} kaolinite peak was similar in frequency to that depicted in Fig. S5b for a low-crystallinity kaolinite (1024 and 999 cm^{-1}), although different to that reported for kaolinite at $\sim 1020 \text{ cm}^{-1}$ (Shao et al. 2018). As a precaution, however, the strong contributions of the three outliers (Sediments C13, C14, and C17) must be considered in the interpretation of the PC1 loading.

Set-2

Figure 3c depicts the PCA scores (PC1 and PC2) for Set-2. Two main outliers were observed: group A (sediments T1 and T2) due to their very high positive PC1 scores. These two samples were visually described as “black ooze” and contained a large amount of fine black semi-liquid material. A further sample B (sediment T5) appeared as an additional outlier along positive PC2. There was a separation of scores into groups C and D along PC2. The loadings for PC1 and PC2 (Fig. 3d) were reversed from those of Set-1, with PC1 loading now dominated by peaks due to organic carbon (2921–2851 cm^{-1}) and kaolinite clay (3695–3620 cm^{-1} and 1003 cm^{-1}), while the loading for PC2 was inversely dominated by carbonate (1448 cm^{-1}). As for Set-1, caution should be exercised in interpretation of PC1 loading due to the high leverage of the sediments T1 and T2 (Parnka Pt. samples).

Prior to the prediction of properties of Set-2 from the Set-1 calibrations, the match between calibration and prediction spectra was tested by comparing their PCA scores to see if there is a likelihood that the spectra used to derive the calibration samples carried the same information as those used for prediction. The Set-2 validation sample spectra were compared with those of the filter-pressed Set-1 calibration samples by projecting their scores onto the Set-1 scores. The PCA score projections are depicted in Fig. 4, showing that the sediments Set-2 T3–T11 scores formed a group at the right-hand boundary of the Set-1 score map, that is, high Set-1 PC1 scores. The sediment T1 scores lay near the left-hand boundary of Set-1 PC1 while sediment T2 scores were near the center of the Set-1 score map. The large separation of the Set-2 T3–T11 samples from the center of the Set-1 score map brings into question the potential reliability of predictions of Set-2 from a Set-1 PLSR calibration, and the appropriateness of such a relatively small Set-1 calibration dataset.

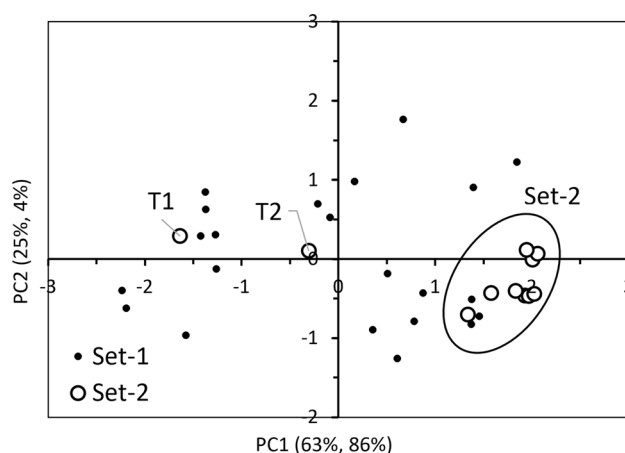


Fig. 4 PCA projection map of PC2 versus PC1 scores for the Set-2 scores (○) projected onto the Set-1 scores (●) using the filter-press method. Grouping of the Set-2 samples is illustrated, and the Parnka Point outliers T1 and T2 are labeled. Scores for the Set-1 samples C13, C14, and C17 were not included in the PCA calculations and removed as outliers

PLSR analysis

Calibration Set-1

Because of the strong correlation between TOC, TP, TN, pH and conductivity in the Coorong (see analytical data cross-correlations in Table S3), it was decided that only TOC analysis would be discussed here. The PLSR cross-validation regression plots for TOC in the Set-1 as-received ATR, filter-pressed ATR, freeze-dried ATR, and freeze-dried DRIFT are depicted in Fig. 5a–d, and statistics presented in Table 2. Outlier sample C12 was omitted from the regressions reported here, except for the DRIFT spectra. The wet as-received Set-1 samples (Fig. 5a) gave only marginal accuracy ($R^2 = 0.78$ and $\text{RMSECV} = 1.12\%$). A strong improvement in regression accuracy ($R^2 = 0.89$ and $\text{RMSECV} = 0.78\%$) was achieved using the filter-press spectra (Fig. 5b). The freeze-dried Set-1 ATR samples (Fig. 5c) resulted in a further slight improvement ($R^2 = 0.95$ and $\text{RMSECV} = 0.51\%$).

Traditionally, the DRIFT technique has been used to predict soil properties with infrared spectroscopy. As the DRIFT method is unsuitable for wet samples, the freeze-dried samples were used to build the DRIFT calibration. A plot of the DRIFT regression for TOC ($R^2 = 0.93$ and $\text{RMSECV} = 0.62\%$) is depicted in Fig. 5d, showing a high accuracy close to that of the freeze-dried ATR. Cross-validation statistics for the Set-1 vis-NIR are also presented in Table 2, showing far lower accuracy ($R^2 = 0.59$ and $\text{RMSECV} = 1.54\%$) compared to any of the ATR MIR results, and required omission of two outliers (C12 and C22). Clearly, dried-powder sample ATR and DRIFT

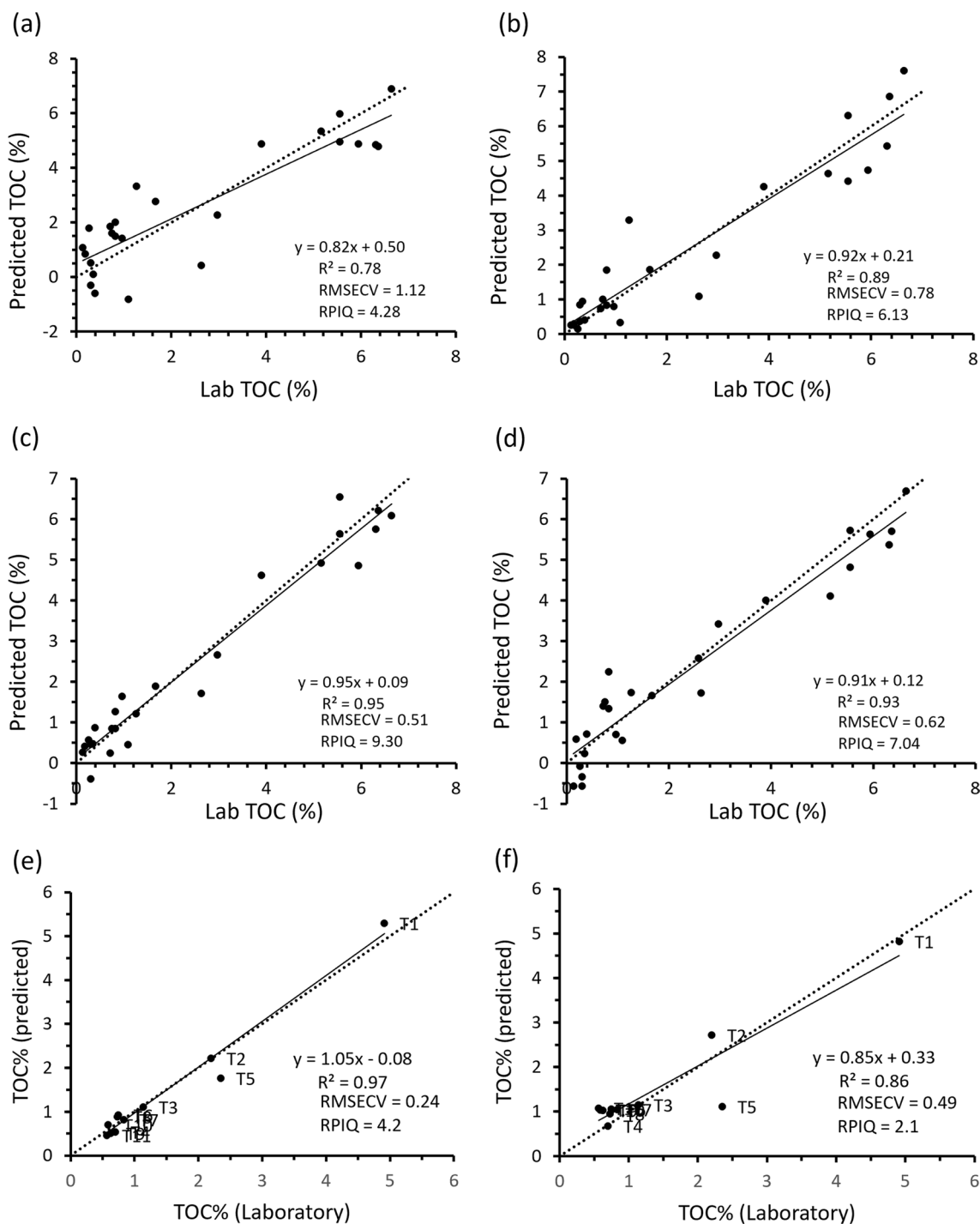


Fig. 5 PLSR cross-validation and predictions for TOC versus laboratory reference values with inset regression statistics; **a** Set-1 as-received ATR, **b** Set-1 filter-pressed ATR, **c** Set-1 freeze-dried ATR, **d** Set-1 freeze-dried DRIFT, **e** Set-2 cross-validation regression, and

f Set-2 predicted from the Set-1 calibration. The 1:1 line is shown (.....) and points are labeled according to sample numbers in Table 2

methods still performed best, but the filter-pressed ATR method accuracy was still acceptable, with the added advantage that it may eventually be used in the field and on wet samples.

Model testing Set-2

A plot of the cross-validation regression of TOC for the filter-pressed Set-2 sediments is presented in Fig. 5e.

Table 2 PLSR prediction statistics for TOC prediction versus laboratory reference data for Set-1 by cross-validation and Set-2 by cross-validation and prediction from the Set-1 calibration

Statistic	As-received ATR	Set-1				Set-2	
		Filter-pressed ATR	Freeze-dried ATR	DRIFT	Vis-NIR Reflectance	Filter-pressed ATR Cross-validation	Filter-pressed ATR Prediction
R^2	0.78	0.89	0.95	0.93	0.59	0.97	0.86
RMSECV	1.12	0.78	0.51	0.62	1.54	0.24	0.49
PLSR Factors	5	5	5	5	5	0	0
Bias	0.05	0.03	-0.04	-0.10	-0.02	5.00	5.00
RPIQ	4.28	6.13	9.30	7.04	3.01	4.25	2.06
Outlier ID	C12	C12	C12		C12, C22		

Outlier ID according to Table 1

Cross-validation accuracy was excellent, with $R^2=0.97$ and $RMSECV=0.24\%$, although the regression was highly leveraged by the three high TOC samples; T1, T2 and T5, and the use of 5 PLSR factors from 11 samples may be considered excessive. In order to get a better assessment of regression robustness, predictions of TOC concentrations for the Set-2 samples were made using the PLSR calibrations derived from the filter-pressed Set-1 samples. The prediction regressions are plotted in Fig. 5f and statistics included in Table 2, including values for R^2 , RMSEP, Bias and RPIQ statistics. The effect of extreme value outliers can be seen by considering the RPIQ values. Since RPIQ is derived from the 1st and 3rd interquartile distances, and ignores the 4th interquartile value, extreme value outliers are effectively removed from this statistic. When outlier samples are not included in the regression statistics, as shown by the relatively low RPIQ values (i.e., $RPIQ < 2$), a far less robust regression is suggested.

Of concern was that the high TOC analyte values for the T1, T2, and T5 sediments had a strong leverage on the regression statistics. The upper two samples (0–2 cm and 8–10 cm) from Parnka Point (sediments T1 and T2) had by far the highest predicted values for all analytes. Sediment T5 was only poorly fitted. Further, the predicted RMSEP value (0.49%) was comparable to the laboratory data values for T6–T11 (0.56–0.83%), resulting in the predicted values of the low TOC in sediments being close to 1%. This suggested that the current Set-1 calibration was incapable of precise predictions of values less than 1%, indicated by the poor fit of the Set-1 and Set-2 spectra according to the score projection in Fig. 4.

Discussion

The surface moisture surrounding the solid particles in the as-received samples was assumed to be distributed as a uniform film on the entire ATR crystal surface, with minimal

contact points for the sediment itself. This film was within the evanescent wave, resulting in the strong water absorbance peak and lack of spectral detail for the sediment components. In this study, we have shown that the filter-press ATR method is a straightforward technique to amplify the spectral signal of solid components in wet samples, circumventing previous problems with excessive water content in infrared analysis. By pressing the wet sample onto the surface of the ATR crystal using a filter paper, the suspended solid material in the slurry is pressed into optical contact with the crystal as a highly concentrated plug, improved the spectral signature of the solids.

Using this ATR method, the TOC predictions were comparable in accuracies reported for dried sample ATR and DRIFT soil samples (Soriano-Disla et al. 2014). If sample oxidation can be avoided by drying, and adequate laboratory facilities are available, then dry powdered samples using either ATR or DRIFT provide the highest accuracy. However, if drying causes chemical changes, then the filter-pressed ATR method provides a useful and convenient alternative for analyzing wet samples. Several potential advantages are demonstrated for the new filter-press ATR method described in our study. First, wet sediment samples can be analyzed rapidly on-site, avoiding the costs and time of transporting large numbers of samples to the laboratory. Analysis can be carried out in a much timelier manner compared to conventional MIR methods and it avoids problematic issues with drying wet sediments that may result in changes in chemistry due to oxidation processes. Second, in-field use of this MIR ATR method, using a portable setup powered by a battery mounted in a vehicle, suggests its potential as a rapid, practical, and accurate alternative to other MIR techniques.

However, there are also a number of potential issues worth discussing with this new method. First, there is the question of how to ensure the consistency of the water content of different samples, and how to eliminate the influence

of sample moisture difference on MIR detection. Moisture in the sediments was likely from three main sources: (1) intra-particle chemically and physically bonded water, (2) interparticle water at field capacity, and (3) excess water due to the fact that the samples were submerged at time of collection. This excess moisture may well be random and, thus, poorly influence the efficacy of infrared regression analysis. In this study, we assume that the Moisture% data in Table 1 represents the intra-particulate water components, and if so, would be highly correlated with TOC ($R^2=0.86$), clay ($R^2=0.90$) and sand content ($R^2=0.91$). PLSR modeling of TOC for the as-received samples was not predicted well (R^2 only 0.78), with the PLSR loading weights characteristic of mainly water, with little indications of organic matter (Fig. 3b). The water component of the as-received samples was, thus, random according to what was detected on the ATR crystal. Not so with the filter-pressed samples, with an R^2 of 0.89. Further, the PLSR loading weights (Fig. 3d) showed strong TOC peaks and minimal water peaks.

The reason for this is that the as-received method mainly sampled the water film in optical contact with the crystal, and less of the sediment solids that would be correlated with TOC. In contrast, the moisture in the filter-pressed sample at the point of sampling on the ATR crystal was low due to the high anvil pressure. In this study, the samples were pressed under the filter and ATR anvil with a force of 18 kg force on an area on the crystal of 2.5 mm², equivalent to a pressure of 70,608 Kpa (706 Bar). This pressure was believed to be sufficient to extract most of the interstitial water (Patila et al. 2017). Spectra of the as-received samples and the distributions in Fig. S6 showed little change in the absorbances of the main water peaks at 3450 cm⁻¹ compared to the filter-pressed samples (Fig. 1a and b).

Another important source of possible prediction error is the within-sample heterogeneity, particularly as the sample area of the ATR crystal used here was only about 2.5 mm². Sample heterogeneity, relevant to the ATR method, can be due to spatial variations in composition throughout the bulk sample, or due to shell fragments in the case of estuarine sediments. Some means of homogenizing or mixing the bulk sediment sample, such as with a portable blender and hand grinding, may be required to reduce spatial heterogeneity and to ensure a uniform sample for reference laboratory and infrared analysis. Further, the optimum number of replicates still needs to be determined to account for sample heterogeneity. Analysis of replicate subsamples could significantly reduce the impact of compositional variations within the bulk sample. In the case of this study, only a single subsample was used, so it is expected that improved prediction accuracy would result from using replicates. This requires further targeted investigation.

The issue of possible significant spectral contamination by the filter paper, although not evident here, cannot

be totally dismissed. This could occur if some of the filter paper may come into optical contact with the ATR crystal and result in the spectrum of the filter paper being superimposed onto the sample spectrum. Filter paper would show up as cellulose, with peaks expected at about 3400, 2900, 1100 cm⁻¹ due to CH₂, C–O, and O–H bonds (d'Halluin et al. 2017). Every effort had been taken to ensure that enough sample had been put onto the crystal to provide sufficient thickness of the sample. Figure 4 confirmed that there was no visual evidence of filter-paper signals in the filter-pressed reference sample scans. However, PCA loading-4 for Set-1 (depicted in Fig. S4) suggested that there may have been some suggestion of minor cellulose C–OH peaks at 3333–3272 cm⁻¹. However, this loading only contributed 2% to the spectral variability, so any impact of such peaks would be minimal. In any case, any small contribution of filter paper is not considered to be a serious problem for multivariate regression analysis such as PLSR, as the TOC PLSR model would most likely only use the spectral information correlating with TOC rather than from random filter-paper contributions.

Prediction errors can also sometimes result when using small calibrations with high degrees of compositional variation between some of the samples, as in Set-1, and poor matching of the Set-2 spectra by Set-1 as illustrated by the lack of coverage of their PCA score projections in Fig. 4. A larger and more inclusive calibration set may alleviate this problem to some extent. Further, the prediction results indicated that accuracy may benefit from using a much larger and more diverse calibration in order to cover the possibility of poor representation of future unknown samples. In the present case, the relatively few calibration samples (26 in total) were taken from a relatively large area, raising the likelihood that the compositional variation with the sites were not fully tested. Attempting to use such a small calibration to predict outside the calibration samples could produce predictions with excessive bias caused by the lack of coverage of their spectra and the differing chemistry between the two data sets. A larger and more inclusive calibration set could alleviate this problem to some extent. In the case of large site like the Coorong, this method could reduce costly laboratory analysis and rapidly highlight where eutrophication (i.e., high TOC, TN, TP) hotspots occur. Additionally, analysis of wet agricultural soils could be readily achieved by this new filter-press method.

Conclusions

We have developed a modified 'filter-press' ATR method that, for the first time, allows direct MIR analysis of TOC and likely other physico-chemical properties in environmental field-moist or saturated sediments without the need for

drying. There is a strong increase in solids spectral intensities by pressing the wet sediment onto an ATR crystal using the filter paper, and PLSR models using this technique resulted in greatly improved accuracy compared to that of the non-pressed as-received field-moist samples, with accuracies comparable to that of dry powder ATR and DRIFT. Our findings confirmed the filter-pressed ATR method as proof-of-concept, demonstrated using TOC analyses of field-wet sediments. This new method potentially reduces the adverse impacts of moisture as one of the major barriers to in-field application of MIR techniques to environmental samples. The portable and rapid analysis ability of the filter-press ATR method could also be utilized to provide information on soil/sediment heterogeneity (e.g., for high-resolution sediment quality mapping purposes) under natural wet environmental conditions. Testing of this capability with a much larger calibration set and validating against a larger and more diverse laboratory dataset is a recommended next step.

Supplementary Information The online version contains supplementary material available at <https://doi.org/10.1007/s12665-023-11350-y>.

Acknowledgements This study used sediment samples collected in the Healthy Coorong Healthy Basin program funded by the South Australian and Australian Governments.

Author contributions All authors contributed to the writing and editing of the paper. Leslie Janik: Sample collection, spectral analysis, design of experiment and first draft of paper Luke Mosley: Planning, sample collection and editing Stuart Simpson: Editing Mark Farrell: Editing All authors have read and approved the final manuscript.

Funding Open access funding provided by CSIRO Library Services.

Data availability All data is available if requested.

Declarations

Conflict of interest The authors declare that there are no ethics or competing interests, and declare that no funds, grants, or other support were received during the preparation of this manuscript. All authors contributed to the writing and editing of the paper. Sample collection and analysis were performed by Luke Mosley and Leslie Janik. The first draft of the manuscript was written by Leslie Janik and all authors commented on previous versions of the manuscript. All authors read and approved the final manuscript.

Open Access This article is licensed under a Creative Commons Attribution 4.0 International License, which permits use, sharing, adaptation, distribution and reproduction in any medium or format, as long as you give appropriate credit to the original author(s) and the source, provide a link to the Creative Commons licence, and indicate if changes were made. The images or other third party material in this article are included in the article's Creative Commons licence, unless indicated otherwise in a credit line to the material. If material is not included in the article's Creative Commons licence and your intended use is not permitted by statutory regulation or exceeds the permitted use, you will need to obtain permission directly from the copyright holder. To view a copy of this licence, visit <http://creativecommons.org/licenses/by/4.0/>.

References

- Baldock JA, Hawke B, Sanderman J, Macdonald LM (2013) Predicting contents of carbon and its component fractions in Australian soils from diffuse reflectance mid-infrared spectra. *Soil Research* 51:577–595. <https://doi.org/10.1071/SR13077>
- Bargrivan S, Smernik R, Fitzpatrick R, Mosley LM (2018) The application of a spectrophotometric method to determine pH in acidic (pH<5) soils. *Talanta*. <https://doi.org/10.1016/j.talanta.2018.04.074>
- Barros TL, Bracewell SA, Mayer-Pinto M, Dafforn KA, Simpson SL, Farrell M, Johnston EL (2022) Wildfires cause rapid changes to estuarine benthic habitat. *Environ Pollut* 308:119571. <https://doi.org/10.1016/j.envpol.2022.119571>
- Bellon-Maurel V, Fernandez-Ahumada E, Palagos B, Roger JM, McBratney A (2010) Critical review of chemometric indicators commonly used for assessing the quality of the prediction of soil attributes by NIR spectroscopy. *Trends Anal Chem* 29(9):1073–1081. <https://doi.org/10.1016/j.trac.2010.05.006>
- Chapkanski S, Ertlen D, Rambeau C, Schmitt L (2020) Provenance discrimination of fine sediments by mid-infrared spectroscopy: calibration and application to fluvial palaeo-environmental reconstruction. *Sedimentology* 67(2):1114–1134. <https://doi.org/10.1111/sed.12678>
- Chapkanski S, Jacq K, Brocard G, Vittori C, Debret M, De Giorgi AU, d'Ottavio D, Giuffr  EM, Goiran JP (2022) Calibration of Short-Wave InfraRed (SWIR) hyperspectral imaging using Diffuse Reflectance Infrared Fourier Transform spectroscopy (DRIFTS) to obtain continuous logging of mineral abundances along sediment cores. *Sed Geol* 428:106062. <https://doi.org/10.1016/j.sedgeo.2021.106062>
- Cohen MJ, Prenger JP, DeBusk WF (2005) Visible-near infrared reflectance spectroscopy for rapid, nondestructive assessment of wetland soil quality. *J Environ Qual* 34:1422–1434. <https://doi.org/10.2134/jeq2004.0353>
- Creepers N, Fitzpatrick R, Shand P (2013) The occurrence of inland acid sulphate soils in the floodplain wetlands of the Murray-Darling Basin, Australia, identified using a simplified incubation method. *Soil Use Manag* 29:130–139. <https://doi.org/10.1111/sum.12019>
- d'Halluin M, Rull-Barrull J, Bretel G, Labrugere C, Le Grogne E, Felpin FX (2017) Chemically modified cellulose filter paper for heavy metal remediation in water. *ACS Sustain Chem Eng* 5(2):1965–1973. <https://doi.org/10.1021/acssuschemeng.6b02768>
- Dematt  JA, Ara ujo SR, Fiorio PR, Fongaro CT, Nanni MR (2015) VIS-NIR-SWIR spectroscopy in soil evaluation along a toposequence in Piracicaba. *Revista Ciencia Agronomica* 46:679–688. <https://doi.org/10.5935/1806-6690.20150054>
- Ehsani MR, Upadhyaya SK, Fawcett WR, Protsailo LV, Slaughter D (2001) Feasibility of detecting soil nitrate content using a mid-infrared technique. *Trans ASAE* 44:1931–1940. <https://doi.org/10.13031/2013.6991>
- Fearn T (2001) Standardisation and calibration transfer for near infrared instruments: a review. *J Near Infrared Spectrosc* 9:229–244. <https://opg.optica.org/jnirs/abstract.cfm?URI=jnirs-9-4-229>
- Gee GW, Bauder JW (1986) Particle-Size Analysis. In: Klute A (ed) *Methods of soil analysis, Part 1. Physical and mineralogical methods*, agronomy monograph No. 9, 2nd edition, American Society of Agronomy/Soil Science Society of America, Madison, WI, 383–411. <https://doi.org/10.2136/sssabookser5.4.c12>
- Geladi P, Kowalski BR (1986) Partial least-squares regression: a tutorial. *Analytica Chimica Acta*, 186 1-17. Oriffiths PR, De Haseth JA (eds) *In Fourier Transform Infrared Spectrometry*, 2nd Edition, (Ed. James D. Winefordner) May3 2007, Ch 15. ISBN: 978-0-471-19404-0.

- Gingele FX, De Deckker P (2005) Clay mineral, geochemical and Sr–Nd isotopic fingerprinting of sediments in the Murray-Darling fluvial system, southeast Australia. *Aust J Earth Sci* 52(6):965–974. <https://doi.org/10.1080/08120090500302301>
- Griffiths PR, de Haseth JA (2007) Fourier transform infrared spectrometry. John Wiley & Sons, Hoboken
- Hahn A, Compton JS, Meyer-Jacob C, Kirsten KL, Lucasssen F, Mayo MP, Schefub E, Zabel M (2016) Holocene paleo-climatic record from the South African Namaqualand mudbelt: a source to sink approach. *Quatern Int* 404:121–135. <https://doi.org/10.1016/j.sedgeo.2021.106062>
- Hume R, Marschner P, Schilling R, Mason S, Mosley LM (2022) Detection of agriculturally relevant lime concentrations in soil using mid-infrared spectroscopy. *Geoderma* 409:115639. <https://doi.org/10.1016/j.geoderma.2021.115639>
- Janik LJ, Keeling JL (1993) FT-IR partial least-squares analysis of tubular halloysite in kaolin samples from the Mount Hope kaolin deposit. *Clay Miner* 28(3):365–378. <https://doi.org/10.1180/claymin.1993.028.3.03>
- Janik LJ, Skjemstad JO (1995) Characterization and analysis of soils using mid-infrared partial least-squares. 2. Correlations with some laboratory data. *Aust J Soil Res* 33(4):637–650. <https://doi.org/10.1071/SR9950637>
- Janik LJ, Merry RH, Skjemstad JO (1998) Can mid infrared diffuse reflectance analysis replace soil extractions? *Aust J Exp Agric* 38:681–696. <https://doi.org/10.1071/EA97144>
- Janik LJ, Skjemstad JO, Shepherd KD, Spouncer LR (2007) The prediction of soil carbon fractions using mid-infrared-partial least square analysis. *Aust J Soil Res* 45:73–81. <https://doi.org/10.1071/SR06083>
- Janik LJ, Soriano-Disla JM, Forrester ST, McLaughlin MJ (2016a) Effects of soil composition and preparation on the prediction of particle size distribution using mid-infrared spectroscopy and partial least-squares regression. *Soil Res* 54:889–904. <https://doi.org/10.1071/SR16011>
- Janik LJ, Soriano-Disla JM, Forrester ST, McLaughlin MJ (2016b) Moisture effects on diffuse reflection infrared spectra of contrasting minerals and soils: a mechanistic interpretation. *Vib Spectrosc* 86:244–252. <https://doi.org/10.1016/j.vibspec.2016.07.005>
- Jovanovski G, Stefov V, Shoptrajanov B, Boev B (2002) Minerals from Macedonia IV. Discrimination between some carbonate minerals by FTIR spectroscopy. *Min Abh* 404:1–13
- Khayamim F, Wetterlind J, Khademi H, Robertson AJ, Cano AF, Stenberg B (2015) Using visible and near infrared spectroscopy to estimate carbonates and gypsum in soils in arid and subhumid regions of Isfahan, Iran. *J near Infrared Spectrosc* 23(3):155–165. <https://doi.org/10.1255/jnirs.1157>
- Koçak A, Wyatt W, Comanescu MA (2021) Comparative study of ATR and DRIFT infrared spectroscopy techniques in the analysis of soil samples. *Forensic Sci Int* 328:1–8. <https://doi.org/10.1016/j.forsciint.2021.111002>
- Kresović M, Jakovljević M, Blagojević S, Žarković B (2010) Nitrogen transformation in acid soils subjected to Ph value changes. *Arch Biol Sci Belgrade* 62(1):129–136. <https://doi.org/10.2298/ABS1001129K>
- Larkin PJ (2018) Instrumentation and sampling methods. In *Infrared and Raman Spectroscopy (Second Edition)*. 2.4.1 Attenuated Total Reflectance. <https://doi.org/10.1016/j.geoderma.2021.115639>
- Linker R, Kenny A, Shaviv A, Singher L, Shmulevich I (2004) Fourier Transform Infrared-attenuated total reflection nitrate determination of soil pastes using principal component regression, partial least squares, and cross-correlation. *Appl Spectrosc* 58:516–520. <https://doi.org/10.1366/000370204774103327>
- Linker R, Shmulevich I, Kenny M, Shaviv A (2005) Soil identification and chemometrics for direct determination of nitrate in soils using FTIR-ATR mid-infrared spectroscopy. *Chemosphere* 61:652–658. <https://doi.org/10.1016/j.chemosphere.2005.03.034>
- Van der Marel HW, Beutelspacher H (1976) Atlas of infrared spectroscopy of clay minerals and their admixtures, pp 70–111, pp 243–247. Elsevier Publishing Company.
- McCarty GW, Reeves JB (2006) Comparison of near infrared and mid infrared diffuse reflectance spectroscopy for field-scale measurement of soil fertility parameters. *Soil Sci* 1712:94–102. <https://doi.org/10.1097/01.ss.0000187377.84391.54>
- McCarty GW, Reeves JB III, Reeves VB, Follett RF, Kimble JM (2002) Mid-infrared and near-infrared diffuse reflectance spectroscopy for soil carbon measurement. *Soil Sci Soc Am J* 66:640–646. <https://doi.org/10.2136/sssaj2002.6400a>
- Melucci D, Zappi A, Poggioli F, Morozzi P, Giglio F, Tositti L (2019) ATR-FTIR spectroscopy, a new non-destructive approach for the quantitative determination of biogenic silica in marine sediments. *Molecules* 24(21):3927. <https://doi.org/10.3390/molecules24213927>. (1–13)
- Merry RH and Fitzpatrick RW (2005) An evaluation of the soils of Tilley Swamp and Morella Basin, South Australia. Cooperative Research Centre for Landscape Environments and Mineral Exploration (CRC LEME) Open File Report 195
- Milosevic M (2004) Internal Reflection and ATR Spectroscopy. *Appl Spectrosc Rev* 39(3):365–384. <https://doi.org/10.1081/asr-200030195>
- Mosley LM, Priestley S, Brookes J, Dittmann S, Farkaš J, Farrell M, Ferguson AJ, Gibbs M, Hipsey M, Huang J, Lam-Gordillo O, Simpson SL, Tyler JJ, Waycott M, Welsh DT (2023) Extreme eutrophication and salinisation in the Coorong estuarine-lagoon ecosystem of Australia's largest river basin (Murray-Darling). *Mar Pollut Bull*. <https://doi.org/10.1016/j.marpolbul.2023.114648>
- Mosley LM, Thomas BP, Fitzpatrick RW (2019) A guide to managing acid sulfate soil risks in south Australian river Murray wetlands. Acid Sulfate Soils Centre, University of Adelaide. Acid Sulfate Soils Centre Report: ASSC_155
- Mosley LM, Priestley S, Brookes J, Dittmann S, Farkaš J, Farrell M, Ferguson AJ, Gibbs M, Hipsey M, Huang J, Lam-Gordillo O (2020) Coorong water quality synthesis with a focus on the drivers of eutrophication. Goyder Inst Water Res Tech Report Ser (20/10)
- Nguyen TT, Janik LJ, Raupach M (1991) Diffuse reflectance infrared Fourier transform (DRIFT) spectroscopy in soil studies. *Soil Research* 29(1):49–67. <https://doi.org/10.1071/SR9910049>
- Oudghiri F, García-Morales JL, Rodríguez-Barroso MR (2014) Rapid screening of estuarine sediments properties Using thermogravimetric analysis and attenuated total reflectance (ATR) by Fourier transform infrared (FTIR) spectrometry. *Water Air Soil Pollut* 225(1853):1–10. <https://doi.org/10.1007/s11270-013-1853-1>
- Patil UD, Puppala AJ, Hoyos LR, Pedarla A (2017) Modeling critical-state shear strength behavior of compacted silty sand via suction-controlled triaxial testing. *Eng Geol* 231:21–33. <https://doi.org/10.1016/j.enggeo.2017.10.011>
- Poulenard J, Perrette Y, Fanget B, Quetin P, Trevisan D, Dorioz JM (2009) Infrared spectroscopy tracing of sediment sources in a small rural watershed (French Alps). *Sci Total Environ* 407(8):2808–2819
- Priestley S, Mosley L, Farkas J, Tyler J Shao, Y, Shanafield M Banks, E Wong, WW, Leyden E (2022) Sources and transport of nutrients in the Coorong. Goyder Institute for Water Research Technical Report Series No. 22/01
- Rayment GE, Lyons DJ (2011) Soil chemical methods: Australasia/George E. Rayment and David J. Lyons. CSIRO Publishing Collingwood, Vic
- Reeves JB III (2010) Near- versus mid-infrared diffuse reflectance spectroscopy for soil analysis emphasizing carbon and laboratory versus on-site analysis: Where are we and what needs to be

- done? *Geoderma* 158:3–14. <https://doi.org/10.1016/j.geoderma.2009.04.005>
- Robertson AHJ, Hill HR, Main AM (2013) International Workshop “Soil Spectroscopy: the present and future of Soil Monitoring” FAO HQ, Rome 4–6 December 2013
- Rosén P, Vogel H, Cunningham L, Reuss N, Conley DJ, Per Persson P (2010) Fourier transform infrared spectroscopy, a new method for rapid determination of total organic and inorganic carbon and biogenic silica concentration in lake sediments. *J Paleolimnol* 43:247–259. <https://doi.org/10.1007/s10933-009-9329-4>
- Shao Y, Farkas J, Holmden C, Mosley L, Kell-Duivesteyn I, Izzo C, Reis-Santos P, Tyler J, Torber P, Fryda J, Taylor H, Haynes D, Tibby J, Gillanders BM (2018) Calcium and strontium isotope systematics in the lagoon estuarine environments of South Australia: implications for water source mixing, carbonate fluxes and fish migration. *Geochim Cosmochim Acta* 239:90–108. <https://doi.org/10.1016/j.gca.2018.07.036>
- Shaviv A, Kenny A, Shmulevitch I, Singher L, Raichlin Y, Katzir A (2003) Direct monitoring of soil and water nitrate by FTIR based FEWS or membrane systems. *Environ Sci Technol* 37(12):2807–2812. <https://doi.org/10.1021/es020885+>
- Shi XZ, Aspandiar M, Oldmeadow D (2014) Reflectance spectral characterization and mineralogy of acid sulphate soil in subsurface using hyperspectral data. *Int J Sediment Res* 29:149–158. [https://doi.org/10.1016/S1001-6279\(14\)60031-7](https://doi.org/10.1016/S1001-6279(14)60031-7)
- Soriano-Disla JM, Janik L, Viscarra-Rossel RA, McDonald LM, McLaughlin MJ (2014) The performance of visible, near and mid infrared spectroscopy for prediction of soil physical, chemical and biological properties. *Appl Spectrosc Rev* 49:139–186. <https://doi.org/10.1080/05704928.2013.811081>
- Soriano-Disla JM, Janik LJ, Forrester ST, Grocke SF, Fitzpatrick RW, McLaughlin MJ (2019) The use of mid-infrared diffuse reflectance spectroscopy for acid sulfate soil analysis. *Stoten* 646:1489–1502. <https://doi.org/10.1016/j.scitotenv.2018.07.383>
- Sullivan L, Ward N, Toppler N, Lancaster G (2018) National acid sulfate soils guidance: national acid sulfate soils identification and laboratory methods manual, Department of Agriculture and Water Resources, Canberra. ACT 1354:991012820975502300
- Turner BL, Newman S, Cheesman AW, Reddy KR (2007) Sample pre-treatment and phosphorus speciation in wetland soils. *Soil Sci Soc Am J* 71:538–1546. <https://doi.org/10.2136/sssaj2007.0017>
- Viscarra Rossel RA, Walvoort DJJ, McBratney AB, Janik LJ, Skjemstad JO (2006) Visible, near infrared, mid infrared or combined diffuse reflectance spectroscopy for simultaneous assessment of various soil properties. *Geoderma* 131:59–75. <https://doi.org/10.1016/j.geoderma.2005.03.007>
- Weidler PG, Friedrich F (2007) Determination of the refractive index of particles in the clay and sub-micrometer size range. *Am Miner* 92(7):1130–1132. <https://doi.org/10.2138/am.2007.2313>
- Xuebin X, Changwen D, Fei M, Yazhen S, Ke W, Dong L, Jianmin Z (2019) Detection of soil organic matter from laser-induced breakdown spectroscopy (LIBS) and mid-infrared spectroscopy (FTIR-ATR) coupled with multivariate techniques. *Geoderma* 355(113905):1–13. <https://doi.org/10.1016/j.geoderma.2019.113905>
- Zimmermann M, Leifeld J, Fuhrer J (2007) Quantifying soil organic carbon fractions by infrared-spectroscopy. *Soil Biol Biochem* 39:224–231. <https://doi.org/10.1016/j.geoderma.2019.113905>

Publisher's Note Springer Nature remains neutral with regard to jurisdictional claims in published maps and institutional affiliations.